Acta Pharmaceutica Sinica B 2018;8(3):420–431

Chinese Pharmaceutical Association
Institute of Materia Medica, Chinese Academy of Medical Sciences

Acta Pharmaceutica Sinica B

www.elsevier.com/locate/apsb
www.sciencedirect.com

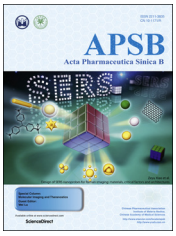

ORIGINAL ARTICLE

Nanoparticles with high payloads of pipemidic acid, a poorly soluble crystalline drug: drug-initiated polymerization and self-assembly approach

Elisabetta Pancani[a], Mario Menendez-Miranda[a], Alexandra Pastor[a,b], François Brisset[c], Marie-Françoise Bernet-Camard[d], Didier Desmaële[b], Ruxandra Gref[a,*]

[a]*Institut de Sciences Moléculaires d'Orsay (ISMO), Univ. of Paris-Sud, Université Paris-Saclay, Orsay 91405, France*
[b]*Institut Galien, UMR8612 Univ. of Paris-Sud, Université Paris-Saclay, Châtenay-Malabry 92290, France*
[c]*Institut de Chimie Moléculaire et des Matériaux d'Orsay (ICMMO), Univ. of Paris-Sud, Université Paris-Saclay, Orsay 91405, France*
[d]*EA4043 "Unité Bactéries Pathogènes et Santé" (UBaPS), Univ. of Paris-Sud, Université Paris-Saclay, Châtenay-Malabry 92290, France*

Received 3 February 2018; received in revised form 28 February 2018; accepted 16 March 2018

KEY WORDS

Pipemidic acid;
Nanoparticle;
Antibiotic;
Nanoprecipitation;
Crystalline drug;
Drug-initiated polymerization

Abstract Nowadays, biodegradable polymers such as poly(lactic acid) (PLA), poly(D,L-lactic-*co*-glycolic acid) (PLGA) and poly(ε-caprolactone) (PCL) remain the most common biomaterials to produce drug-loaded nanoparticles (NPs). Pipemidic acid (PIP) is a poorly soluble antibiotic with a strong tendency to crystallize. PIP incorporation in PLA/PLGA NPs was challenging because of PIP crystals formation and burst release. As PIP had a poor affinity for the NPs, an alternative approach to encapsulation was used, consisting in coupling PIP to PCL. Thus, a PCL–PIP conjugate was successfully synthesized by an original drug-initiated polymerization in a single step without the need of catalyst. PCL–PIP was characterized by NMR, IR, SEC and mass spectrometry. PCL–PIP was used to prepare self-assembled NPs with PIP contents as high as 27% (*w/w*). The NPs were characterized by microscopy, DLS, NTA and TRPS. This study paves the way towards the production of NPs with high antibiotic payloads by drug-initiated polymerization. Further studies will deal with the synthesis of novel polymer–PIP conjugates with ester bonds between the drug and PCL. PIP can be considered as a model drug and the strategy developed here could be extended to other challenging antibiotics or anticancer drugs and employed to efficiently incorporate them in NPs.

*Corresponding author. Tel.: +33 1 69158234.
E-mail address: ruxandra.gref@u-psud.fr (Ruxandra Gref).

Peer review under responsibility of Institute of Materia Medica, Chinese Academy of Medical Sciences and Chinese Pharmaceutical Association.

https://doi.org/10.1016/j.apsb.2018.03.008

1. Introduction

By 2050, infections due to resistant bacteria are expected to become the leading cause of death, overcoming cancer[1]. The increasing spread of resistant pathogens is a consequence of systematic use, and sometimes misuse, of antimicrobial agents. Intracellular bacteria are among the most life threatening ones because of their ability to "hide" inside the cells of a living organism, invade even the cells of the immune system and survive in active and/or latent forms[2–4].

To fight against this threat, new strategies are required to administrate antimicrobial agents in an optimized manner. One of the most promising approaches is the development of biodegradable and biocompatible nanocarriers to efficiently load antibiotics, protect them from degradation and target them to infection sites. Encapsulation allows circumventing limitations such as low solubility of the drug, tendency to crystallize, inability to cross cell membrane and unfavorable biodistribution. This could possibly reduce toxic side effects and increase patient's compliance[2].

Quinolones are one of the most successful families of antibiotics, both from economical and clinical point of view. Discovered fortuitously more than 50 years ago, they are orally and parenterally active against a broad spectrum of bacteria[5,6]. They exert their antibacterial action by formation of a ternary complex between the DNA and DNA gyrase (topoisomerase II) or topoisomerase IV (enzymes involved in the supercoiling and underwinding of DNA, respectively) consequently blocking their action and therefore inhibiting bacterial DNA replication. However, first generation quinolones are no longer used in therapy because of their unfavorable physicochemical profiles, lower tissue penetration and narrower antibacterial spectrum in comparison to the following generations of quinolones[7]. Nanotechnology could offer a tremendous opportunity to recycle these "old" drugs and give them a new life by delivering them in an optimized manner[8–10].

Pipemidic acid (PIP), a pyridopyrimidine quinolone, is an example of such drugs which could benefit from encapsulation in nanoparticles (NPs). PIP showed better activity on intracellular bacteria such as *Pseudomonas aeruginosa*, *Escherichia coli* and *Salmonella typhimurium* (*S. typhimurium*) than nalidixic and piromidic acid which are structurally related first generation quinolones[11–13]. However, PIP possesses a very low aqueous solubility[14] and a strong tendency to crystallize which make its administration very challenging and limit its therapeutic applications.

Interestingly, it has been described that PIP can form supramolecular complexes with native β-cyclodextrins (CDs) thus improving its apparent solubility and stability in water[15]. The same authors demonstrated a higher antibacterial activity of the PIP:CDs complexes against *E. coli* and *Staphylococcus aureus* in comparison to free PIP. Indeed, the complexes allowed to improve the solubility of PIP in water and possibly enhanced PIP transport through membranes thus improving the inhibition of DNA replication by the drug.

However, contrary to NPs, CD complexes do not offer the possibility to control drug release or to target infection sites. Indeed, nanotechnology revolutionizes drug delivery by achieving: i) controlled delivery of drugs to (intracellular) targets; ii) transcytosis of drugs across biological barriers and iii) possibility to visualize the sites of drug delivery (theranostics)[16]. Nowadays, biodegradable NPs made of polyesters such as poly(lactic acid) (PLA), poly(D,L-lactic-*co*-glycolic acid) (PLGA) and poly(ε-caprolactone) (PCL) remain the most employed in the field of drug delivery[17–19]. Fluoroquinolones such as levofloxacin, ciprofloxacin and ofloxacin were successfully incorporated in PLGA micro- and nanoparticles to achieve sustained release and improve the drug retention/uptake inside infected cells[20–23].

Here we describe the challenges related to the incorporation of PIP in PLA/PLGA NPs using the standard physical encapsulation methods, nanoemulsion and nanoprecipitation, which are shown to be associated to drug crystallization, burst release and poor encapsulation. The reasons for the unsuccessful encapsulation of PIP using these techniques are analyzed. In the light of these findings, a different approach was envisaged. PIP was covalently linked to PCL following an original drug-initiated polymerization procedure, devoid of catalysts. The resulting PCL–PIP copolymer definitively avoided the drawbacks of PIP incorporation in NPs, *i.e.*, drug leakage during NP formation and crystallization. PCL–PIP was thoroughly characterized by ^{1}H and ^{13}C NMR, IR and mass spectrometry to unambiguously characterize its structure. Furthermore, PCL–PIP was successfully used to prepare self-assembled NPs. Noteworthy, the PIP content in the NPs was as high as 27% (*w*/*w*). The NPs were comprehensively characterized by a set of complementary techniques: dynamic light scattering (DLS), NP tracking analysis (NTA) and tunable resistive pulse sensing (TRPS). Finally, the degradation of PCL–PIP was investigated *in vitro*.

2. Material and methods

2.1. Chemicals

Poly(lactic) acid (PLA) ester-terminated (MW = 10–18 kDa) (PLA1), PLA acid-terminated (MW = 18–24 kDa) (PLA2), poly (vinyl alcohol) (PVA-88% hydrolyzed), sodium cholate and pipemidic acid (PIP) and ϵ-caprolactone were purchased from Sigma–Aldrich (Saint-Quentin Fallavier, France). PLGA 50:50 acid terminated (MW = 42–65 kDa, 10P001) (P1), PLGA 75:25 acid terminated (MW = 5–20 kDa, 10P015) (P15), PLGA 50:50 ester terminated (MW = 70–100 kDa, 10P016) (P16), PLGA 50:50 acid terminated (MW = 5–20 kDa, 10P019) (P19) and PLGA 75:25 ester terminated (MW = 10–25, 10P033) (P33) were kindly provided by PCAS (Expansorb, Aramon, France).

Injectable water was purchased from Cooper (Melun, France), while dichloromethane (DCM-Analar Normapur) and methanol (MeOH) were from Prolabo (Fontenay-sous-bois, France). The solvents were analytical grade. KCl (99%) was purchased from Alfa Aesar (Karlsruhe, Germany). Lipase from *Pseudomonas cepacia* (30 U/mg) and proteinase K from *Tritirachium album* were purchased from Sigma–Aldrich (Saint-Quentin Fallavier, France). Chemicals obtained from commercial suppliers were used without further purification.

Diethyl ether and tetrahydrofuran (THF) were distilled from sodium/benzophenone ketyl. Methanol was dried over magnesium and distilled under a nitrogen atmosphere. All reactions involving air- or water-sensitive compounds were routinely conducted in glassware which was flame-dried under a positive pressure of nitrogen or argon.

2.2. General

IR spectra were obtained as solid on a Fourier Transform Bruker Vector 22 spectrometer. Only significant absorptions are listed. The ^{1}H and ^{13}C NMR spectra were recorded on Bruker Avance 300 (300 MHz and 75 MHz, for ^{1}H and ^{13}C, respectively) spectrometers. Recognition of methyl, methylene, methine, and quaternary carbon nuclei in ^{13}C NMR spectra rests on the J-modulated spin-echo sequence. Analytical thin-layer chromatography was performed on Merck silica gel 60F254 glass precoated plates (0.25 mm layer). Column chromatography was performed on Merck silica gel 60 (230–400 mesh ASTM).

2.3. PCL–PIP synthesis and characterization

Pipemidic acid (384 mg, 1.26 mmol) in a glass tube was dissolved in freshly distilled ϵ-caprolactone (5.0 g, ~45 mmol) by gentle heating. The homogeneous mixture was degassed through three freeze-pump-thaw cycles and the glass tube was heated under argon to 210 °C (Wood's alloy bath) for 6 h. After cooling, the mixture was taken up into THF (20 mL) and precipitated with petroleum ether (*c.a.* 60 mL). The mixture was centrifuged (11,000 × *g*) for 5 min. The supernatant was discarded and the precipitation process was repeated twice. The obtained residue was dried under vacuum at 80 °C for 1 h. The waxy brown solid was taken in DMSO and freeze dried to leave a light brown soft powder (1.2 g, 66%). IR (neat) 3600–3400, 2933, 2865, 1739, 1725, 1629, 1599, 1561, 1542, 1514, 1476, 1445, 1433, 1419, 1396, 1382, 1357, 1349, 1291, 1279, 1263, 1236, 1198, 1156, 1123, 1100, 1087, 1015, 987, 962, 841, 813, 737, 714 cm^{-1}; ^{1}H NMR (300 MHz, DMSO-d_6) δ 14.75 (s, 1H, CO_2H), 9.21 (s, 1 H, H-5), 8.97 (s, 1H, H-2), 4.40 (q, J = 6.9 Hz, 2H, NCH_2CH_3), 4.33 (t, J = 4.8 Hz, 1H, CH_2OH)), 3.98 (m, 25H, $CH_2CH_2OCOCH_2$, CH_2NCH_2), 3.61 (br s, 4H, CH_2NCH_2), 3.36 (dt, J = 5.8 Hz, J = 6.0 Hz, 2H, CH_2OH), 2.37 (t, J = 7.2 Hz, 2H, $NCOCH_2$), 2.27 (t, J = 7.2 Hz, 19H, $OCOCH_2CH_2CH_2CH_2CH_2O$), 1.70–1.23 (m, 70H, $COCH_2CH_2CH_2CH_2CH_2O$, NCH_2CH_3) ppm; ^{13}C NMR (75 MHz, DMSO-d_6) δ 177.16 (C, C-4), 172.79 (nC, $CH_2CO_2CH_2$), 170.88 (C, CON), 165.24 (C, C-7), 160.70 (C, CO_2H), 160.19 (CH, C-5), 155.08 (C, C-8a), 150.75 (CH, C-2), 109.68 (C, C-3), 108.68 (C, C-4a), 63.52 (nCH_2, CH_2OCOCH_2), 60.57 (CH_2, CH_2CH_2OH), 45.95 (CH_2, NCH_2CH_3), 44.02 ($2CH_2$, $N(CH_2CH_2)_2N$), 43.69 ($2CH_2$, $N(CH_2CH_2)_2N$), 33.60 (CH_2, $NCOCH_2CH_2$), 33.39 (nCH_2, $OCOCH_2CH_2CH_2CH_2CH_2O$), 32.19 (CH_2, CH_2CH_2OH), 28.07 (CH_2, $OCOCH_2CH_2CH_2CH_2CH_2O$), 27.84 (nCH_2, $OCOCH_2;CH_2CH_2CH_2CH_2O$), 25.23 ($CH_2$, $OCOCH_2CH_2CH_2CH_2CH_2O$), 25.09 (CH_2, $OCOCH_2CH_2CH_2CH_2CH_2O$), 24.93 (nCH_2, $OCOCH_2CH_2CH_2CH_2CH_2O$), 24.46 (CH_2, $OCOCH_2CH_2CH_2CH_2CH_2O$), 24.36 (CH_2, $OCOCH_2CH_2CH_2CH_2CH_2O$), 24.12 (nCH_2, $OCOCH_2CH_2CH_2CH_2CH_2O$), 14.38 (CH_3, NCH_2CH_3) ppm.

Despite the fact that the polymerization occurred at relatively high temperature, no decomposition was observed in the NMR spectra (^{1}H or ^{13}C). In fact, pipemidic acid is a highly stable compound and the heating was done under nitrogen atmosphere after careful removing oxygen using three freeze-pump-thaw cycles. Previously reported thermogravimetric analysis showed that no decomposition of pipemidic acid occurred before 259 °C[24]. In addition, the purity and the dispersity of PCL–PIP were characterized by size exclusion chromatography (SEC) employing polystyrene standards, THF as eluent and a mixed LT3000 column (Malvern Panalytical, UK).

2.4. Synthesis of decarboxylated caprolactone adduct 4

To pipemidic acid (151 mg, 0.5 mmol) in a glass tube was added freshly distilled ϵ-caprolactone (70 mg, 0.60 mmol). The heterogeneous mixture was degassed through three freeze-pump-thaw cycles and the glass tube was heated under argon to 250 °C (Wood's alloy bath) for 4 h. After cooling, the mixture chromatographed on silica gel elution with CH_2Cl_2/MeOH, 10:1 to give 45 mg of compound **4** .^{1}H NMR (300 MHz, DMSO-d_6) δ 8.96 (s, 1H, H-5), 7.90 (d, J = 8.1 Hz, 1H, H-2), 5.98 (d, J = 8.1 Hz, 1H, H-3), 4.16 (q, J = 7.1 Hz, 2H, NCH_2CH_3), 3.95-3.90 (m, 4H, NCH_2), 3.57 (br. s, 4H, NCH_2), 2.35 (t, J = 7.6 Hz, 2H, $NCOCH_2$), 1.55–1.25(m, 6H, $COCH_2CH_2CH_2CH_2CH_2O$), 1.29 (t, J = 7.1 Hz, 3H, NCH_2CH_3) ppm.

2.5. Nanoparticle preparation

2.5.1. Nanoemulsion method

Biodegradable PLA/PLGA nanoparticles (NPs) were prepared by an oil-in-water emulsion method using PVA as a surfactant. First, an amount of polymer ranging from 20 to 75 mg was dissolved into a volume of DCM between 1 and 1.5 mL. This polymer solution was mixed to PIP (from 2 to 7.5 mg) and an adequate amount of MeOH (0.2–0.4 mL) was added to solubilise the PIP. All PLA/PLGA polymers and various PIP/polymer ratios were studied for PIP incorporation in NPs. The organic phase was poured into 4 mL of injectable water containing 0.5% or 1% *w/v* PVA (or sodium cholate) and vortexed for 20 s. The mixture was sonicated using a probe (Sonopuls HD 2070, BANDELIN electronic GmbH & Co., Berlin, Germany) at 20% power for 1.5 min and for 30 additional seconds at 10% in an ice bath to avoid overheating. Alternatively, the oil-in-water emulsion was formed by homogenisation (WiseTis homogeniser, Wids, Germany) at 50% of the instrument power for 1.5 min. In all cases, the organic solvent was evaporated at room temperature under gentle magnetic stirring. Control empty NPs were prepared in the same conditions, except that PIP was not added.

The preparation of PCL–PIP NPs was also carried out by oil-in-water emulsion. Briefly, 20 mg of PCL–PIP polymer (or a 50:50 mixture of PCL–PIP and PLGA at 10 mg/mL each) were solubilised in 1.5 mL of DCM. This organic phase was mixed to 4 mL of 0.5% or 1% *w/v* PVA (or sodium cholate) injectable water, vortexed for 20 s and sonicated in ice bath as already described. Organic solvent was then evaporated at room temperature under gentle magnetic stirring.

2.5.2. Nanoprecipitation method

An amount of polymer ranging from 25 to 75 mg was solubilised in 2.5 mL of acetone. The polymer solution was added to PIP powder (2.5–7.5 mg). As PIP is poorly soluble in acetone, 0.2–0.5 mL MeOH was added to completely solubilize the drug. All polymers and different PIP/polymer ratios were studied. The organic phase was added drop-wise into 5 mL of 0.5% PVA aqueous (injectable water)

solution under continuous vigorous magnetic stirring leading to the instantaneous precipitation of the polymer under the form of NPs. The organic solvent was then evaporated at room temperature under gentle magnetic stirring. Duration of solvent evaporation was controlled. Control empty NPs were prepared in the same conditions, except that PIP was not added.

2.6. Nanoparticle characterization

The presence of crystals and aggregates in the formulations was assessed by observing the NP suspensions with a Zeiss Primo Vert™ inverted optical microscope (Carl Zeiss AG, Oberkochen, Germany) equipped with an Axiocam camera. An aliquot of NPs was withdrawn under magnetic stirring and deposited in a Malassez chamber for cell counting to obtain a likely uniform distribution of eventual aggregates and crystals on the glass surface.

SEM images were acquired on a Zeiss SUPRA 55 VP field emission gun scanning electron microscope. It was set to a low voltage (1 kV) and low currant (a few pA) in order not to damage the samples and to avoid and any conductive coating that could bother direct observation of the samples. Secondary electron type detector was used to record the images.

2.6.1. Size measurement by DLS and zeta potential measurement

The mean hydrodynamic diameter of all NPs was measured by DLS with an equilibration time of 60 s using a Malvern Zetasizer® (Nano ZS90, Malvern Instruments S.A., Worcestershire, UK). Measurements were performed at least in triplicate. Sample dilutions with injectable water were performed according to ISO 22412. The values obtained at 100 times dilutions are given in Table 1. All autocorrelation functions have an intercept with amplitude equal to 0.9 or higher. Mean diameters were reported as Z average (nm) ± SE (standard error - with a PdI lower than 0.1) or as number mean diameter (nm) ± SD (standard deviation, nm) (Table 1).

2.6.2. Size distribution and concentration measurements by NTA

The average hydrodynamic diameter and the concentration of the NPs was determined at 25 °C by Nanoparticle Tracking Analysis (NTA, NanoSight LM10, Malvern Instruments S.A., Worcestershire, UK) after a 10,000 times dilution in injectable water. Each sample was measured 3 times, consisting of 5 runs of 60 s each (at least 4000 completed tracks for each run). Results were reported as mean diameter (nm) ± SD (nm) and as particles/mL ± RSD% (relative standard deviation). NPs concentration was calculated by the instrument by counting the NPs in a known volume of suspension (100 µm × 80 µm × 10 µm)[25], hence allowing the extrapolation of the number of particles per mL.

2.6.3. Size measurement by TRPS (Izon) and concentration quantification

Additionally, the mean hydrodynamic diameter and the concentration of NPs samples were measured by TRPS (qNano Gold, Izon Science Ltd, Oxford, UK) after a 500 times dilution of the sample in 0.03% Tween 20 filtrated PBS solution. TRPS use a Coulter-type counter to measure directly NPs size and concentration. The NPs cross one by one a small pore in a membrane filled with an electrolyte, causing changes in the ionic current flow which is generated by the applied voltage. Such current changes induce blockade events with amplitudes denoted as the blockade magnitude. The blockade magnitude is proportional to particle size, which can be accurately measured after calibration with known standards. Each NPs sample was run at least in triplicate. The pulse signal of the instrument was calibrated with a 110 nm polystyrene particle standard supplied by Izon Science and diluted 1000 times in the same solvent used for samples. The membrane pore size used (NP150, Izon Science) was rated for 70–420 nm particles. A 47 mm stretch and a potential of 0.7 V were applied to the pore. The measurements were performed with at least 1000 particles being detected for each run.

Results were reported as mean diameter (nm) ± SD (nm) and as particles/mL ± RSD%.

2.7. Drug quantification

To determine the amount of PIP or PIP–COOMe effectively incorporated in the PLA/PLGA NPs, the NPs suspensions were centrifuged at 17,000 × g for 20 or 40 min depending on the NPs size. Aliquots of the supernatants were withdrawn to assess the quantity of non-encapsulated drug (D_s). Aliquots of the original NPs suspension were withdrawn and DMSO was added in order to dissolve the NPs. Thus, the total amount of drug (D_t) present in the NP formulations was determined by HPLC quantification. The amount of encapsulated drug (D_e) was calculated as in Eq. (1):

$$D_e = D_t - D_s \quad (1)$$

All the samples were dosed by reverse-phase HPLC (RP-HPLC) after dilution in a mixture acetonitrile/water 45/55 (*v/v*) using a Agilent HPLC system (Agilent 1100 Series) equipped with a C18 column (Kinetex 5 µ C18, 100 A, Phenomenex) and UV detector at λ = 280 nm for PIP and at λ = 260 nm for PIP–COOMe. The chromatographic conditions were set as follows: solvent A 0.1% trifluoroacetic acid (TFA) in water and solvent B 0.1% TFA in acetonitrile; 0–2 min: 0–20% B, 2–6 min: 20–45% B, 6–10 min: 45–75% B, 10–15 min: 75–0%. Flow rate: 1.0 mL/min at room temperature. The injection volume was set at 10 µL. In all cases, R^2 values were higher than 0.99. From the obtained data the

Table 1 Hydrodynamic mean diameter and concentration of PCL–PIP NPs. NPs average diameter was determined by DLS, NTA and TRPS. For DLS measurements data are reported as number distribution to allow the comparison with NTA and TRPS results. Concentration results correspond to the concentration (NP/mL) in the NP original suspensions. The measures were performed after 10,000 times dilution for NTA and 500 times dilution for TRPS to meet both instruments requirements. RSD (%), relative standard deviation.

NP	PVA (%, *w/w*)	Size distribution (nm ± SD)			Concentration (NP/mL ± RSD%)	
		DLS Number distribution	NTA	TRPS	NTA	TRPS
100% PCL–PIP	0.5	215 ± 72	130 ± 37	126 ± 52	0.74×10^{13} ± 3%	1.19×10^{13} ± 12%
100% PCL–PIP	1	183 ± 51	134 ± 31	112 ± 35	1.02×10^{13} ± 8%	2.18×10^{13} ± 14%
50% PCL–PIP + 50% PLGA	0.5	214 ± 64	136 ± 42	121 ± 45	0.83×10^{13} ± 2%	1.56×10^{13} ± 14%

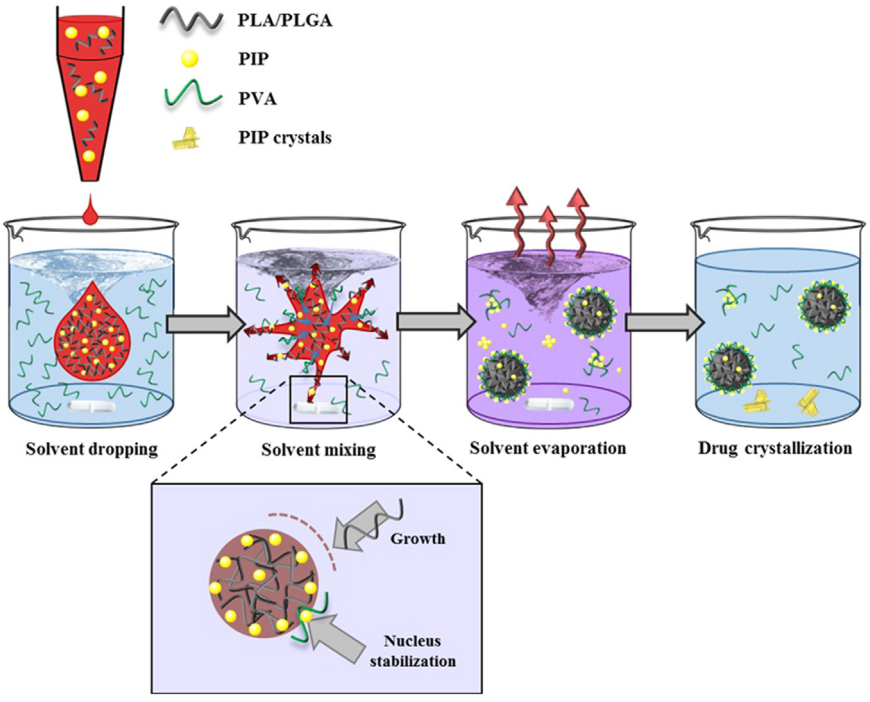

Figure 1 Schematic representation of nanoprecipitation process to obtain PLA/PLGA PIP-loaded NPs. The organic phase (red) containing the polymer (PLA/PLGA) and PIP is poured dropwise into an aqueous solution (blue) containing PVA as surfactant, under vigorous magnetic stirring. Once the drop enters in contact with the aqueous phase, the two solvents are mixed together (purple color) causing the "explosion" of the organic solvent drop. The local fluctuations in the supersaturated system containing the polymer and PIP led to the spontaneous formation of nucleation sites. If the nuclei further encounter more polymer chains, newly formed NPs tend to grow (lower panel). When the polymer concentration decreases, the probability of NP growth decreases too. When the nuclei encounter PVA molecules, PIP and PVA associate at the nucleus surface stopping its growth and leading to a stabilization effect, eventually leading to NP formation. Finally, NP suspension is maintained under magnetic stirring to allow organic solvents evaporation. In turn, solvent evaporation decreases PIP solubility in the suspension medium. PIP molecules which are not stabilized neither on the NPs surface by association to PVA nor by free PVA, crystalize at the bottom of the vial.

DL (defined as the mass fraction of a NP that is composed of drug) was calculated as shown in Eq. (2):

$$\text{DL}\ (\%) = \left(\text{mg of encapsulated drug}/\text{mg of polymer}\right) \times 100 \quad (2)$$

2.8. *Biological tests*

2.8.1. *Bacterial strain and culture*

The experiments herein utilized *Salmonella typhimurium* (subsp. Enterica), strain SL1344, which was a gift from B.A.D. Stocker (Standford University, Stanford, California, USA). Cultures were grown in 10 mL of Luria–Bertani (LB) media (BD Difco™) overnight at 37 °C under gentle shaking.

2.8.2. *Susceptibility test*

The overnight grown bacteria were diluted in PBS to 1.5×10^8 bacteria/mL (0.5 McFarland) according to Antibiogram Committee of French microbiology society guidelines. The bacteria suspension was then used to flood the Petri dishes containing 20 mL of LB agar (prepared with 20 mL of LB Agar Miller formulation, Amresco, USA). The excess of bacterial solution was removed from the dish and discarded. Nitrocellulose disks (diameter = 9 mm, Whatman® Schleicher & Schuell®), previously impregnated with 50 µL of a solution of PIP (solution DMSO/water) to obtain an antibiotic charge of 20 µg/disk, were applied firmly on the agar surface within 15 min of inoculation of the plates. A maximum of 4 disks/plate was applied to avoid possible overlapping of the inhibition zones. The bacteria were considered sensitive to the antibiotic for an inhibition diameter $\geq$ 19 mm[26]. The strain used in this study was sensitive to PIP as the inhibition diameter was 24.5 $\pm$ 0.7 mm.

2.8.3. *PCL–PIP enzymatic degradation assay*

5.95 µL of a PCL–PIP solution in DMSO (10 mg/mL PCL–PIP = 2.10 mg/mL PIP) were added to a 200 µL PBS solution containing: 2.68 U/µL (concentration obtained by adapting a previously published method[27]) or 15 U/mL of lipase (30 U/mg) and/or 7.5 or 15 U/mL of proteinase K. Different concentration combination of the two enzymes were tested. Equivalent amounts (6.25 µL of a 2 mg/mL PIP in DMSO) PIP were used for every enzymes combination as positive controls.

These solutions were incubated for 6, 24 or 48 h at 37 °C. Then, 50 µL of each solution were used to impregnate nitrocellulose disks and applied to petri dishes inoculated with *S. typhimurium* (as already explained in Section 2.8.1). The dishes were incubated for 12 h at 37 °C to allow bacterial growth.

3. Results and discussion

PIP acid is a zwitterionic compound with a very low (0.322 mg/mL) solubility in water[14,15] and strong tendency to form crystals. Drugs with such physico-chemical characteristics are particularly challenging to be incorporated in NPs[28–31]. For

instance, busulfan and ethionamide formed crystals in the NPs suspension medium, which were very difficult to remove, hampering their biomedical applications. An ideal nanocarrier for crystalline drugs such as PIP should: i) have a reproducible monodisperse size distribution; ii) display drug loading (DL) higher than 10% (*w*/*w*); iii) avoid drug crystallization; iv) do not display burst-release of the incorporated drug upon dilution and v) maintain its physicochemical characteristics during storage.

3.1. *Physical incorporation*

To address the challenges of PIP incorporation, NPs were firstly formulated by the most common methods, nanoemulsion and nanoprecipitation, using a series of PLA and PLGA (co)polymers (PLA1, PLA2, P1, P15, P16, P19, P33, see polymer characteristics in method Section 2.1) with different characteristics (molecular weights, lactic:glycolic acid molar ratios and ester or carboxylic terminal groups).

3.1.1. *Nanoemulsion method*

A series of PLA/PLGA NPs containing PIP were prepared by nanoemulsion using a mixture of dichloromethane (DCM) and methanol (MeOH) to solubilize both the polymers and PIP (see materials and methods section). This organic phase was then poured into an aqueous solution containing the surfactant (poly (vinyl alcohol) = PVA) and the two phases were emulsified by sonication. Different PIP% (*w*/*w*) in the polymers (from 0 up to 20%) was studied.

All tested polymers could successfully form monodisperse NPs with sizes ranging from 200 to 270 nm (*Z* average determined by DLS) with a polydispersity index (PdI) lower than 0.1. Even if these formulations could reach DL of 2%–9% (*w*/*w*), the formation of PIP crystals could not be avoided (Supplementary Fig. S1) and burst-release was observed after NP dilution in water (see Supplementary Information).

These findings suggested: i) a preferential localization of PIP on the surface of NPs, as already reported for other drugs with a similar propensity to form crystals[27,32,33] and ii) a low affinity between PIP and the polymers used to prepare the NPs. Most likely, PIP has stronger affinity for PVA, the surfactant that stabilizes the NPs, than for the polymeric matrices. The replacement of PVA with other surfactants such as sodium cholate, whatever the experimental conditions, led to even lower DL and induced NPs aggregation during storage. A probable preferential location of PIP at the NP's surface could be responsible of the burst effect as it has been reported in other cases[27,33].

PIP crystallization could be avoided by using homogenization instead of sonication to obtain the emulsion. However, as less energy was employed to produce the oil-in-water emulsion, considerably larger and polydisperse NPs were formed as compared to sonication. For example, NPs prepared using P19 had mean diameters of 440 nm (DLS *Z* average). The highest PIP loadings (DL of 3.5%, *w*/*w*) were obtained using P19. However, PIP was again released with a burst effect upon dilution.

3.1.2. *Nanoprecipitation method*

The unsatisfactory results obtained by nanoemulsion prompted us to use an alternative method to formulate the particles, nanoprecipitation. PLA/PLGA NPs were prepared by pouring dropwise under vigorous magnetic stirring an acetone and methanol mixture, containing the polymer and PIP, in an aqueous one containing a surfactant (Fig. 1).

Depending mostly on the polymer used, its concentration, the PIP/polymer ratio and surfactant concentration, nanoprecipitation allowed tuning NPs mean size in a wider range (110–270 nm) than nanoemulsion (200–270 nm) while maintaining the PdI of the single formulations lower than 0.1 (indicating their narrow distribution). Interestingly, these results are also in agreement with the size ($d = 164 \pm 27$ nm) and round shape obtained by scanning electron microscopy (SEM, see Supplementary Fig. S2 for an example of typical images). Moreover, in the same experimental conditions, the blank NPs had considerably higher sizes than the loaded ones. For example, empty P19 NPs were around 50–60 nm larger than the PIP loaded ones (see Supplementary Information). Possibly, PIP plays a role as a co-surfactant, reducing the size of the NPs.

Highest DL (11%, *w*/*w*) were obtained with P33 at a 15:100 PIP/P33 ratio (*w*/*w*) in the preparation procedure and at a final PIP concentration of 1.5 mg/mL in water. However, part of PIP crystallized in the formulations. Moreover, an important burst release was observed, as in case of NP obtained by nanoemulsion. For example, NP diluted 50 times in water contained only 2.5 ± 0.5% (*w*/*w*) PIP. These findings support the preferential location of PIP at the NPs surface, as hypothesized in the case of NP made by nanoemulsion.

On the other hand, P19 demonstrated an ability to avoid the formation of crystals until a maximum PIP/P19 ratio of 1:10. However, the DL was very low (around 1%, *w*/*w*) and PIP was found to be located mostly in the supernatant. Indeed, the measured concentration of PIP in the suspension media was 1.5 mg/mL, 5 times more than the water solubility of PIP in water (around 0.3 mg/mL). This solubility increase is possibly due to the formation of PIP/PVA micelles as schematically hypothesized in Fig. 1. This observation is in line with previous studies showing that the surfactant used to produce NPs by nanoprecipitation can also form micelles in the suspension media[32,34,35]. These findings highlight once more the affinity between PIP and PVA which probably contributed to solubilize the drug.

In conclusion, PIP and PVA play key roles in NP formation. Nanoprecipitation takes place by a nucleation and growth mechanism (Fig. 1). When a solvent droplet containing the polymer and PIP is poured in the aqueous phase (polymer non-solvent solution), the solvent diffuses and mix with the aqueous phase. The concentration of the polymer solute in the resulting solution exceeds its thermodynamic solubility limit, leading to supersaturation. When supersaturation is reached, nuclei are spontaneously formed from local fluctuations in the concentration of the solute. Homogeneous supersaturation requires that the mixing of aqueous and organic phases and the associated molecular diffusion of components occurs extremely rapidly as compared to the rate of NPs nucleation. Nuclei grow by sticking other solute molecules from the surrounding solution until the concentration of the still-dissolved solute decreases to the equilibrium concentration[36].

In these processes, NPs stabilization by surfactants plays a crucial role. The NPs growth is arrested by surfactant adsorption and sometimes surfactant moieties can be kinetically trapped inside the NPs' cores during their formation[36]. In a similar way, PIP could act as co-surfactant with PVA cooperatively impeding the growth process. These considerations could explain the difference in size between PIP-loaded and blank NPs, all the experimental parameters being identical.

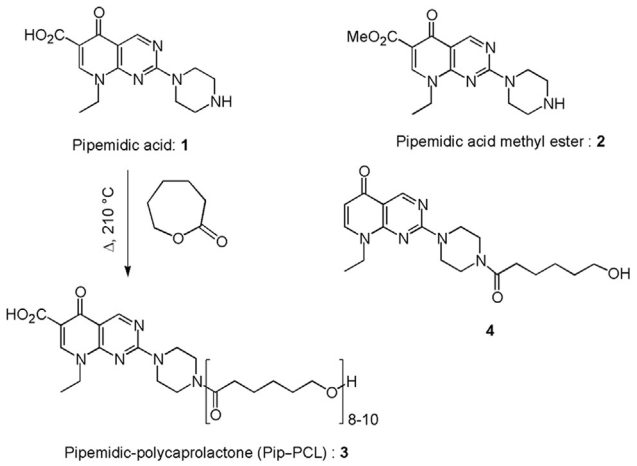

Figure 2 Chemical structures and synthetic pathways. Synthesis of the pipemidic-polycaprolactone (PCL–PIP) **3** from pipemidic acid (PIP) **1** and chemical structure of pipemidic acid derivatives:pipemidic acid methyl ester (PIP–COOMe) **2** and decarboxylated caprolactone adduct **4**.

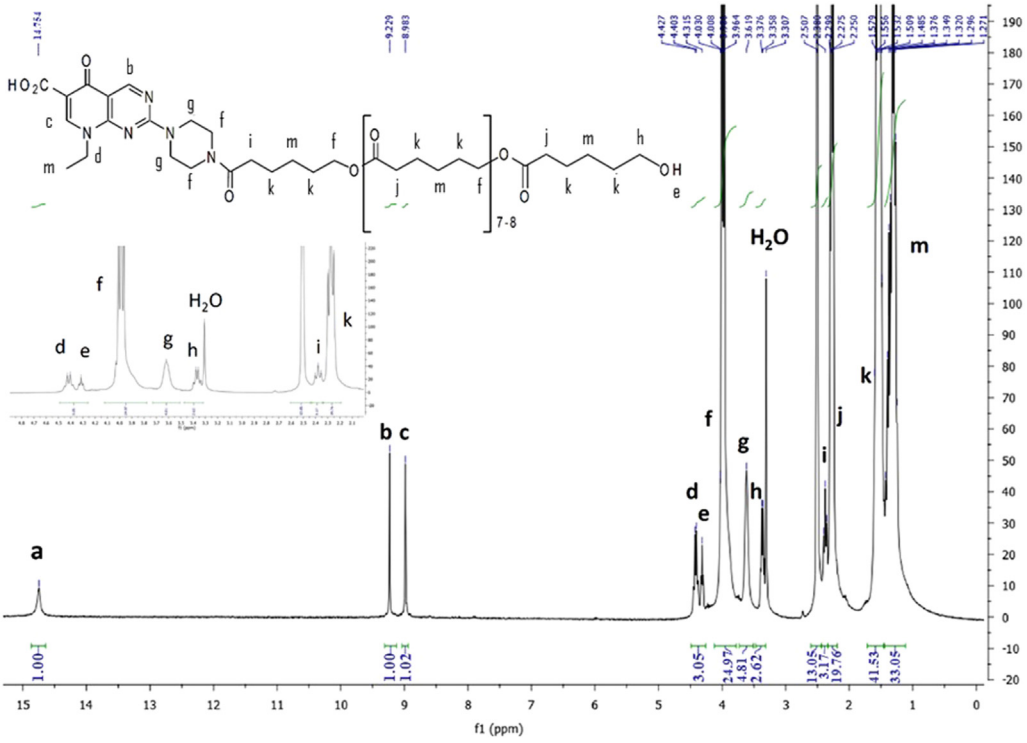

Figure 3 ^{1}H NMR spectrum of PCL–PIP in DMSO-d_6.

Moreover, given its presumed co-surfactant action, PIP should be prone to localize at the NPs' surface, thus explaining the observed burst release. The remaining fraction of PIP in the suspension media could be either stabilized in solution by PVA or crystallized. PIP crystallization occurs in the evaporation step, when the organic solvents (acetone and methanol) are removed, as a consequence of a dramatic PIP solubility decrease in the suspension medium.

Finally, to overcome the bottleneck related to PIP crystallization, incorporation at molecular level has been investigated using NPs made of polymeric β-CD (pCD). Indeed, these NPs already proved their ability to increase the apparent water solubility of challenging crystalline drugs such as tamoxifen, benzophenone and ethionamide without the need of organic solvents[28,31,37]. The pCD NPs were reported to entrap drugs more efficiently than native β-CDs thanks to the confined microdomains inside the crosslinked polymer which are available for drug hosting[38]. However, in the case of PIP, the loadings were lower than 1%, *w/w*.

3.2. *Self-assembly prodrug approach*

As the physical encapsulation of PIP in NPs was unsatisfactory, a different strategy was employed. PIP was chemically modified in an attempt to: i) increase its affinity for the polymeric NPs and ii) avoid crystallization. The *O*-methylated form of PIP (PIP–COOMe, **2**, Fig. 2) was obtained by a simple

esterification reaction using trimethylsilyldiazomethane[39]. This derivative completely avoided PIP crystallization, but the loadings remained very low (lower than 1%).

In this context, the most promising strategy was to graft PIP to a biodegradable polymer to form a conjugate self-assembling under the form of NPs. Drug-initiated polymerization was used to produce in a single step the conjugate, avoiding the use of catalyst. Therefore, poly(ε-caprolactone) (PCL) was the polymer of choice as it has been previously shown that it can polymerize in a controlled manner without catalysts[40]. Moreover, by adjusting the reaction parameters, monodisperse polymers with controlled molecular weights could be obtained.

3.2.1. *Chemical synthesis and characterisation of PCL and PIP conjugate*

The coupling of PIP (Compound **1**, Fig. 2) to PCL was initially attempted through amide bond formation from an already prepared PCL polymer. However, all trials to perform such post-synthetic functionalization turned out to be fruitless whatever the coupling agent used. Therefore, a different synthetic strategy was conceived based on the ring-opening polymerization reaction of ε-caprolactone initiated by the PIP itself. The "drug-initiated" method which consists of using drugs as initiators for the polymerization, has been proposed to prepare well defined polymer prodrugs, using either native functional groups for ring-opening polymerization or pre-functionalized drugs for reversible deactivation radical polymerization techniques[41–44]. Pioneering studies were carried on in this field by Tong and Cheng[45]. On that basis, PIP was heated at 210 °C for 6 h with an excess of ε-caprolactone (~40 equiv.). After precipitation and freeze drying, this reaction produced a light brown soft powder (Fig. 2).

The obtained product was then analyzed by ^{1}H NMR which indicated an average molecular weight of M_n = 1200 g/mol corresponding to 10 caprolactone units for one PIP initiator. ^{1}H NMR spectrum of the product is shown in Fig. 3 where are visible the characteristics peaks of the repeating unit of PCL at 3.98, 2.27, 1.54 and 1.25 ppm. The PCL–PIP polymer was further analyzed by SEC using polystyrene standards. The number average molar mass was M_n = 1730 g/mol and the weight average molar mass was MW = 2160 g/mol indicating a polydispersity of 1.25. However, whereas SEC could indicate the obtention of a unique product with a relatively low polydispersity, ^{1}H NMR was more adapted for composition determination as no standards with different chemical composition are needed.

Since both the carboxylic acid group and the piperazine free amino group could potentially initiate the polymerization, the structure of the obtained polymer was thoroughly characterized by ^{1}H and ^{13}C NMR (Supplementary Fig. S3), IR and mass spectrometry. A band at 1629 cm^{-1} in the IR spectrum (Supplementary Fig. S4) indicated an amide bond in line with the preferential attack of the PCL chain to the piperazine group. Such a strong band is not present in a 10:1 physical mixture of polycaprolactone and PIP (Supplementary Fig. S5). The broad singlet at 14.75 ppm can be attributed to a free carboxylic acid whereas the triplets at 4.32 and 3.26 ppm would possibly be assigned to the hydroxyl proton and the methylene of a terminal CH_2OH group. Observation of signals at 9.21 and 8.97 ppm from the H-2 and H-5

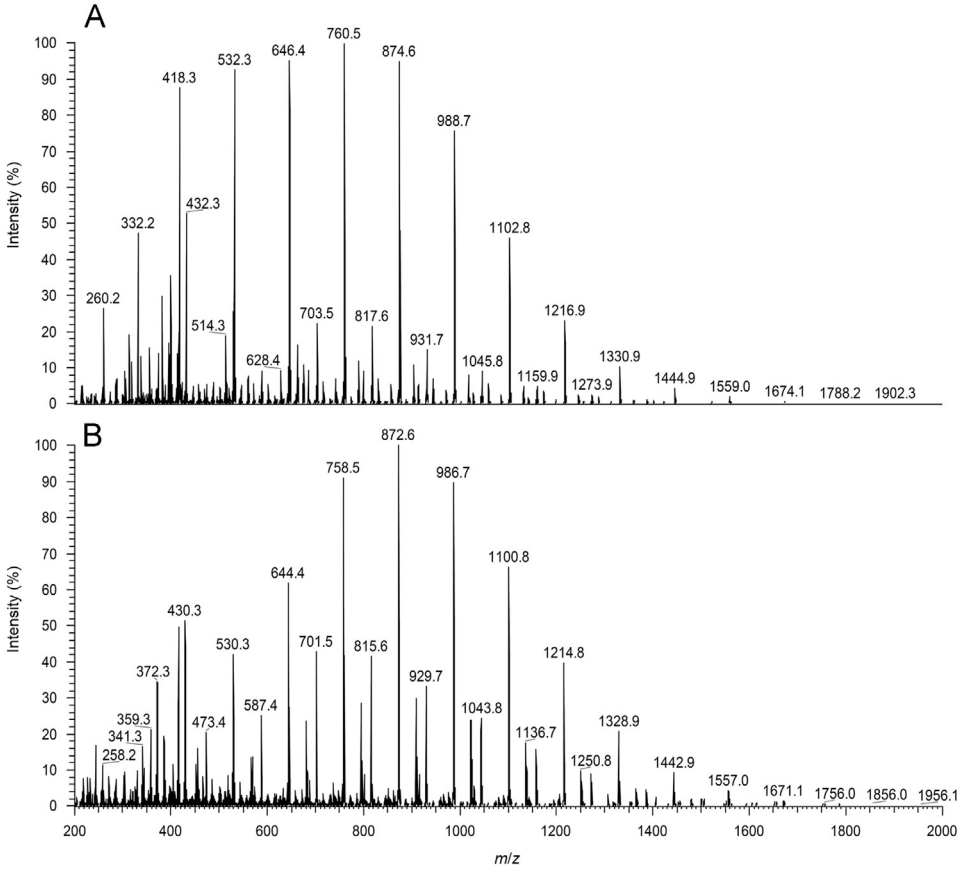

Figure 4 APCI spectrum of the PCL–PIP in acetonitrile. (A) positive mode; (B) negative mode.

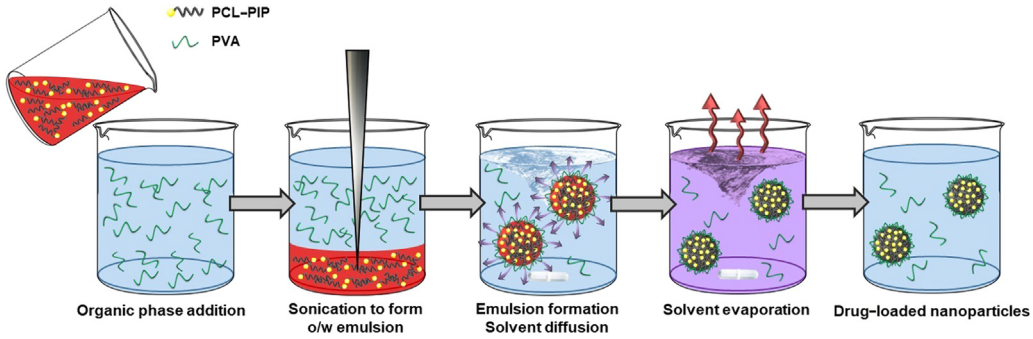

Figure 5 Schematic rapresentation of PCL–PIP NPs formulation by nanoemulsion. The organic phase (red), non-miscible to water and containing the PCL–PIP prodrug, is poured in the aqueous solution containing PVA. The two solvents are then emulsified by sonication forming an oil in water (o/w) emulsion. The hydrophobic PCL–PIP locates in the organic droplets which are stabilized by PVA to avoid coalescence. The NPs suspension is stirred to allow solvent evaporation. Eventually, monodisperse NPs were formed devoid of PIP crystals.

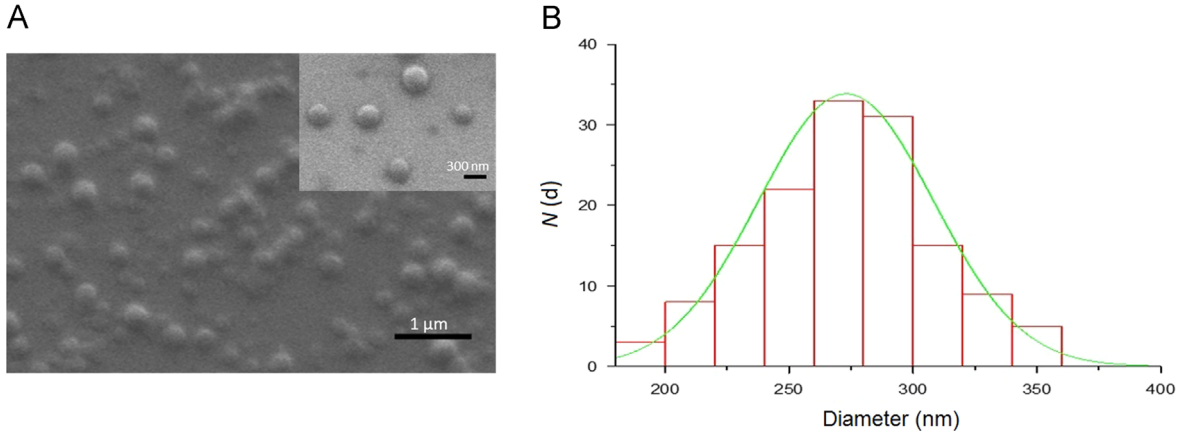

Figure 6 PCL–PIP NPs observed by SEM. a, SEM micrograph; b, histogram of the size distribution of the NPs showing a mean diameter $d = 273 \pm 36$ nm. N(d) refers to the total counts. The scale bar in panel a corresponds to 1 µm while the one of the zoomed region correspond to 300 nm.

protons confirmed the presence of the unchanged pyrido[2,3-*d*] pyrimidine core of PIP. Definitive elucidation of the chemoselectivity of the process was provided by reaction of PIP with 1 equiv. of ε-caprolactone at 240–250 °C for 1 h. In these conditions, concomitant decarboxylation took place giving rise to adduct **4** (Fig. 2) which was unambiguously identified by ^{1}H NMR (Supplementary Fig. S6). In this compound devoid of carboxylic acid, the caprolactone moiety is necessarily bound on the piperazine ring. The observation of the same pattern in the ^{1}H NMR for the proton system around the piperazine ring at 3.89–3.57 ppm for both the PCL–PIP and compound **4**, definitively establish the chemoselectivity of the polymerization process. The use of primary amine as initiator in ε-caprolactone polymerization, though not very common, has been previously reported occurring smoothly using aluminum or tin derivatives as catalyst[46,47].

To complete the PCL–PIP characterization, APCI (+) mass spectrum of the polymer prodrug was registered and it is shown in Fig. 4.

The mass spectrum contains two major features. Firstly, singly charged molecular ion species corresponding to m/z = [Pip + n (CL) + H)]$^+$ are observed from m/z = 418.3 to 1674.1, maximizing at m/z 760.6. Secondly, there are an additional discrete envelope of peaks (703.5, 817.6, 931.7, 1045.8, 1159.9) which correspond to dimeric species ions carrying 2 charges according to the formula [2Pip + (2n + 1) (CL) + 2H]$^{2+}$. The same trend is observed in negative APCI mode.

In conclusion, PCL–PIP was successfully obtained by drug-initiated polymerization of ε-caprolactone and the chemical structure of PIP was unaffected by the reaction conditions. Reproducibly, the synthesized copolymer contained 8 to 10 caprolactone units for one PIP initiator.

3.2.2. *Formulation of PCL–PIP prodrug nanoparticles*

The freshly synthesized PCL–PIP polymer was tested for its capability to self-assembly under the form NPs. Whatever the experimental conditions, nanoprecipitation of PCL–PIP always led to the formation of aggregated NPs. In contrast, nanoemulsion method (Fig. 5) was successful in leading to the formation of NPs devoid of any aggregates. SEM investigations showed that the obtained NPs had a spherical shape and low polydispersity (Fig. 6). However, contrary to PLGA NPs (Supplementary Fig. S2) the PLC–PIP NPs looked flattened on the sample holder. It is worth mentioning that DCM efficiently solubilized the PCL–PIP prodrug, thus avoiding the addition of MeOH as in previous studies.

Interestingly, it was also possible to obtain NPs from blends of PCL–PIP and PLGA/PLA. The most promising formulations, devoid of any aggregates, were composed of 100% PCL–PIP (samples 1 and

2) or of a 50:50 mixture of PCL–PIP and P19 (sample 3). Samples 1 and 2 differed for the amount of PVA used to stabilise the NPs, 0.5% and 1% (*w/w*), respectively. These NPs were thoroughly characterised by using three independent techniques (Table 1).

Table 1 shows that the PCL–PIP mean diameters determined by NTA and TRPS are in good agreement (*i.e.* 130 ± 37 and 126 ± 52 nm, respectively, for sample 1). Of note, the determined concentrations of the NPs suspensions were in agreement too. The size of NPs made of blends of PCL–PIP and PLGA was similar to the one of 100% PCL–PIP NPs.

The average hydrodynamic diameter obtained by DLS was higher than the one obtained by NTA and TRPS. Indeed, DLS values can be biased by the presence of large NPs, which scatter more light than the small ones, thus shifting the size distribution towards higher values. Similar observations were previously reported[28]. Conversely, NTA and TRPS share the particularity of analysing each particle one by one, even if they are based on completely different analysis methods, and thus determined more accurately the hydrodynamic diameter of the NPs.

Nanoparticle Tracking Analysis (NTA) tracks NPs individually in their Brownian motion in order to determine their diffusion coefficient and consequently calculate their sphere-equivalent hydrodynamic diameter using Stokes-Einstein equation. As a consequence, unlike DLS, this technique is independent from the refractive index of the material that composes NPs and therefore cannot lead to overestimation of their size.

By comparing the concentration determined by NTA and TRPS, it can be noticed from Table 1 that the three formulations are in the same order of magnitude (10^{13}). However, a factor of around two between the concentrations measured by these techniques could be due to the different methods of measurement and different dilution factors (10,000 and 500 for NTA and TRPS, respectively) needed to carry on the experiments.

Significant differences were observed when comparing NPs sizes estimated by SEM (Fig. 6) and the ones obtained by the different techniques summarized in Table 1 (DLS, NTA and TRPS). Such differences can be explained by the fact that PCL–PIP NPs may suffer from an alteration of their size caused by the sample preparation required for SEM measurement. Indeed, PCL–PIP NPs still displayed a round shape but they appeared to be flattened on the support surface, as previously described, thus explaining the bigger (*i.e.*, 273 ± 36 nm for sample 2) mean NPs size obtained by analysing SEM images (Fig. 6). Actually, this same effect does not seem to happen in the case of PIP-loaded PLGA NPs, which maintained their spherical shape (see Supplementary Fig. S2), although the same sample preparation was used for both type of particles. Consequently, this "flattened" effect could be ascribable to different physico-chemical properties (glass transition and melting temperatures) of the PLGA and the PCL–PIP polymers.

In a nutshell, NPs, devoid of PIP crystals and containing PIP amounts as high as 27% (*w/w*) were successfully obtained. Their mean diameters of around 130 nm were determined by two independent techniques, NTA and TRPS, which analyze the NPs one by one. The PCL–PIP NPs satisfied the requirements defined in Section 2. They were stable upon 10 days storage and these studies are to be completed with long-term stability investigations.

3.2.3. *PIP susceptibility test and PCL–PIP degradation study on S. typhimurium*

It was interesting to study the stability of the formulated NPs *in vitro*. To evaluate the antimicrobial activity of the PCL–PIP conjugate, a strain (SL1344) of the intracellular bacteria *S. typhimurium* was selected. Indeed, *Salmonella,* an opportunistic gram negative pathogen, is one of the four key global causes of diarrheal diseases with 550 million people falling ill every year[48]. Although non-typhoidal *Salmonella*'s serovars most typically cause uncomplicated gastroenteritis, they can lead to severe consequences in youngs, elderlies and patients with impaired immune system[48–50] requiring the use of antibiotics and patient's hospitalization[51].

The sensitivity of *S. typhimurium* SL1344 to PIP was firstly evaluated. SL1344 resulted sensitive to PIP (inhibition diameter of 24.5 ± 0.7 mm) and was therefore employed to establish the activity of degraded PCL–PIP. To obtain the degradation of the PCL chain, the conjugate was incubated with two enzymes, pseudomonas lipase and proteinase K, used independently or in association. Indeed, the first enzyme was demonstrated to efficiently hydrolyze PCL upon incubation[27,52–54] while the second is commonly used to degrade aliphatic polymers[55]. Unfortunately, as expected, the PCL–PIP conjugate could not be completely degraded by enzymes because of the presence of the tertiary amide linkage between the PIP and the last PCL unit of the conjugate and preventing the activity of the PIP. Indeed, the only natural amino acid, proline, which forms tertiary amide bond in proteins is hydrolyzed by a very specific enzyme (prolidase)[56,57]. In this context, further studies will deal with the synthesis of novel polymer–PIP conjugates, where the drug will be covalently bound through an ester bond to the PCL polymer chain in order to enable an effective drug release and the re-establishment of its antibacterial activity. To this aim, after protection of the terminal NH bond with a suitable group, a diol linker will be added to the acid function of pipemidic in order to take advantage of the well documented alcohol initiated tin catalyzed ring opening polymerization of caprolactone[58]. Studies are underway to elaborate NPs using novel PIP polymer conjugates obtained by drug-initiated polymerization.

4. Conclusions

PIP a poorly soluble antibiotic with a strong tendency to crystallize was poorly entrapped in biodegradable NPs and was burst-released upon the dilution of the NP suspensions. To achieve stable NPs with high PIP payloads, the drug was directly conjugated to the polymers. An original drug-initiated polymerization was employed. The PCL–PIP NPs contained around 27% (*w/w*) PIP. However, PIP was conjugated to through a tertiary amide to a caprolactone unit, making this bond difficult to be enzymatically degraded. Further studies are focused now on the synthesis of novel PCL–PIP conjugates able to be intracellularly degraded to release PIP. Moreover, PIP could be considered as a model drug and the strategy developed here could be extended to other challenging crystalline drugs and employed to enable their efficient incorporation in NPs. With further investigations, the strategy presented here could be extrapolated to other drugs and could find potential applications in the preparation of NPs with high drug payloads for the treatment of severe diseases such as cancer and infections.

Acknowledgments

Financial support for this work was provided by the European Community through the Marie Curie ITN CycloN Hit Grant no.

608407. This work was supported by a public grant overseen by the French National Research Agency (ANR) as part of the "Investissements d'Avenir" program (Labex NanoSaclay, reference: ANR-10-LABX-0035) and by the ANR-14-CE08-0017 grant. We greatly acknowledge PCAS for the donation of PLA and PLGA polymer samples. We thank Prof. Ph. Roger (ICMMO, Orsay) for kind help with SEC analysis.

Appendix A. Supporting information

Supplementary data associated with this article can be found in the online version at https://doi.org/10.1016/j.apsb.2018.03.008.

References

1. O'Neill J. Tackling drug-resistant infections globally: final report and recommendations—the review on antimicrobial resistance [cited 2017 Aug 21]. Available at: ⟨https://amr-review.org/sites/default/files/160525_Finalpaper_withcover.pdf⟩.
2. Ladavière C, Gref R. Toward an optimized treatment of intracellular bacterial infections: input of nanoparticulate drug delivery systems. *Nanomedicine* 2015;**10**:3033–55.
3. Spellberg B, Gilbert D. *Rising plague: the global threat from deadly bacteria and our dwindling arsenal to fight them*. NewYork, NY: Prometheus Books; 2009.
4. Bhavsar AP, Guttman JA, Finlay BB. Manipulation of host-cell pathways by bacterial pathogens. *Nature* 2007;**449**:827–34.
5. Mitscher LA. Bacterial topoisomerase inhibitors: quinolone and pyridone antibacterial agents. *Chem Rev* 2005;**105**:559–92.
6. Oliphant CM, Green GM. Quinolones: a comprehensive review. *Am Fam Physician* 2002;**65**:455–64.
7. Andriole VT. The quinolones: past, present, and future. *Clin Infect Dis* 2005;**41**:S113–9.
8. Mishra RK, Segal E, Lipovsky A, Natan M, Banin E, Gedanken A. New life for an old antibiotic. *ACS Appl Mater Interfaces* 2015;**7**:7324–33.
9. Morachis JM, Mahmoud EA, Almutairi A. Physical and chemical strategies for therapeutic delivery by using polymeric nanoparticles. *Pharmacol Rev* 2012;**64**:505–19.
10. Falagas ME, Grammatikos AP, Michalopoulos A. Potential of old-generation antibiotics to address current need for new antibiotics. *Expert Rev Anti Infect Ther* 2008;**6**:593–600.
11. Shimizu M, Takase Y, Nakamura S, Katae H, Minami A, Nakata K, et al. Pipemidic acid, a new antibacterial agent active against Pseudomonas aeruginosa: *in vitro* properties. *Antimicrob Agents Chemother* 1975;**8**:132–8.
12. Hirai K, Aoyama H, Irikura T, Iyobe S, Mitsuhashi S. Differences in susceptibility to quinolones of outer membrane mutants of *Salmonella typhimurium* and *Escherichia coli*. *Antimicrob Agents Chemother* 1986;**29**:535–8.
13. Fonseca I, Martínez-Carrera S, García-Blanco S. Structure of pipemidic acid. *Acta Cryst Sec C* 1986;**42**:1618–21.
14. Zhang CL, Wang Y. Aqueous solubilities for ofloxacin, norfloxacin, lomefloxacin, ciprofloxacin, pefloxacin, and pipemidic acid from (293.15 to 323.15) K. *J Chem Eng Data* 2008;**53**:1295–7.
15. Iacovino R, Rapuano F, Caso JV, Russo A, Lavorgna M, Russo C, et al. β-Cyclodextrin inclusion complex to improve physicochemical properties of pipemidic acid: characterization and bioactivity evaluation. *Int J Mol Sci* 2013;**14**:13022–41.
16. Abed N, Saïd-Hassane F, Zouhiri F, Mougin J, Nicolas V, Desmaële D, et al. An efficient system for intracellular delivery of β-lactam antibiotics to overcome bacterial resistance. *Sci Rep* 2015;**5**:13500.
17. Anderson JM, Shive MS. Biodegradation and biocompatibility of PLA and PLGA microspheres. *Adv Drug Deliv Rev* 2012;**64**:72–82.
18. Farokhzad OC, Langer R. Impact of nanotechnology on drug delivery. *ACS Nano* 2009;**3**:16–20.
19. Petros RA, DeSimone JM. Strategies in the design of nanoparticles for therapeutic applications. *Nat Rev Drug Discov* 2010;**9**:615–27.
20. Kumar G, Sharma S, Shafiq N, Khuller GK, Malhotra S. Optimization, *in vitro–in vivo* evaluation, and short-term tolerability of novel levofloxacin-loaded PLGA nanoparticle formulation. *J Pharm Sci* 2012;**101**:2165–76.
21. Jeong YI, Na HS, Seo DH, Kim DG, Lee HC, Jang MK, et al. Ciprofloxacin-encapsulated poly(D,L-lactide-*co*-glycolide) nanoparticles and its antibacterial activity. *Int J Pharm* 2008;**352**:317–23.
22. Hua X, Tan S, Bandara HM, Fu Y, Liu S, Smyth HD. Externally controlled triggered-release of drug from PLGA micro and nanoparticles. *PLoS One* 2014;**9**:e114271.
23. Marslin G, Revina AM, Khandelwal VK, Balakumar K, Sheeba CJ, Franklin G. PEGylated ofloxacin nanoparticles render strong antibacterial activity against many clinically important human pathogens. *Colloids Surf B Biointerfaces* 2015;**132**:62–70.
24. Sakon A, Sekine A, Uekusa H. Powder Structure Analysis of Vapochromic Quinolone Antibacterial Agent Crystals. *Cryst. Growth Des.* 2016;**16**:4635–45.
25. Carr B, Wright M. NanoParticle Tracking Analysis. *NanoSight Ltd* 2010;**44**:1–193.
26. Sociéte Francaise de Microbiologie. Comité de l'antibiogramme de la Societé Française de Microbiologie - Recommandations 2013. SFM - EUCAST 1–63 (2013).
27. Chawla JS, Amiji MM. Biodegradable poly(ε-caprolactone) nanoparticles for tumor-targeted delivery of tamoxifen. *Int. J. Pharm.* 2002;**249**:127–38.
28. Costa-Gouveia J, et al. Combination therapy for tuberculosis treatment: pulmonary administration of ethionamide and booster co-loaded nanoparticles. *Sci. Rep.* 2017;**7**:5390.
29. Layre A-M, et al. Busulfan loading into poly(alkyl cyanoacrylate) nanoparticles: Physico-chemistry and molecular modeling. *J. Biomed. Mater. Res. Part B Appl. Biomater.* 2006;**79B**:254–62.
30. Bouligand J, et al. Busulphan-loaded long-circulating nanospheres, a very attractive challenge for both galenists and pharmacologists. *J. Microencapsul.* 2007;**24**:715–30.
31. Daoud-Mahammed S, et al. Cyclodextrin and polysaccharide-based nanogels: Entrapment of two hydrophobic molecules, benzophenone and tamoxifen. *Biomacromolecules* 2009;**10**:547–54.
32. Kumar G, et al. *In vitro* physicochemical characterization and short term *in vivo* tolerability study of ethionamide loaded PLGA nanoparticles: potentially effective agent for multidrug resistant tuberculosis. *J. Microencapsul.* 2011;**28**:717–28.
33. Brigger I, et al. Tamoxifen encapsulation within polyethylene glycol-coated nanospheres. A new antiestrogen formulation. *Int. J. Pharm.* 2001;**214**:37–42.
34. Lannibois H, Hasmy A, Botet R, Chariol O. Surfactant limited aggregation of hydrophobic molecules in water. *J. Phys. II EDP Sci* 1997;**7**:319–42.
35. Gaucher G, Marchessault RH, Leroux J-C. Polyester-based micelles and nanoparticles for the parenteral delivery of taxanes. *J. Control. Release* 2010;**143**:2–12.
36. Lepeltier E, Bourgaux C, Couvreur P. Nanoprecipitation and the 'Ouzo effect': Application to drug delivery devices. *Adv. Drug Deliv. Rev.* 2014;**71**:86–97.
37. Davis ME, et al. Evidence of RNAi in humans from systemically administered siRNA via targeted nanoparticles. *Nature* 2010;**464**:1067–70.
38. Wankar J, et al. Efficient loading of ethionamide in cyclodextrin-based carriers offers enhanced solubility and inhibition of drug crystallization. *Int. J. Pharm* 2017 http://dx.doi.org/10.1016/j.ijpharm.2017.05.041.
39. Hashimoto N, Aoyama T, Shioiri T. New methods and reagents in organic synthesis. 14. A simple efficient preparation of methyl esters with trimethylsilyldiazomethane (TMSCHN2) and its application to

gas chromatographic analysis of fatty acids. *Chem. Pharm. Bullettin* 1981;**29**:1475–8.
40. Gref R, Rodrigues J, Couvreur P. Polysaccharides grafted with polyesters: novel amphiphilic copolymers for biomedical applications. *Macromolecules* 2002;**35**:9861–7.
41. Tong R, Cheng J. Controlled synthesis of camptothecin−polylactide conjugates and nanoconjugates. *Bioconjug. Chem.* 2010;**21**:111–21.
42. Tong R, Cheng J. Drug-initiated, controlled Ring-Opening polymerization for the synthesis of polymer–drug conjugates. *Macromolecules* 2012;**45**:2225–32.
43. Yin Q, et al. Drug-initiated Ring-Opening polymerization of *O*-carboxyanhydrides for the preparation of anticancer drug–poly(*O*-carboxyanhydride) nanoconjugates. *Biomacromolecules* 2013;**14**:920–9.
44. Nicolas J. Drug-initiated synthesis of polymer prodrugs: combining simplicity and efficacy in drug delivery. *Chem. Mater.* 2016;**28**:1591–606.
45. Tong R, Cheng J. Paclitaxel-initiated, controlled polymerization of lactide for the formulation of polymeric nanoparticulate delivery vehicles. *Angew. Chemie Int. Ed* 2008;**47**:4830–4.
46. Dubois P, Degee P, Jerome R, Teyssie P. Macromolecular engineering of polylactones and polylactides. 8. Ring-opening polymerization of ε-caprolactone initiated by primary amines and trialkylaluminum. *Macromolecules* 1992;**25**:2614–8.
47. Hua C, Peng S-M, Dong C-M. Synthesis and characterization of linear-dendron-like poly(ε-caprolactone)-*b*-poly(ethylene oxide) copolymers *via* the combination of Ring-Opening polymerization and Click Chemistry. *Macromolecules* 2008;**41**:6686–95.
48. WHO. WHO | Salmonella (non-typhoidal). World Heal. Organ. (2016).
49. Beceiro A, Tomas M, Bou G. Antimicrobial resistance and virulence: a successful or deleterious association in the bacterial world?. *Clin. Microbiol. Rev.* 2013;**26**:185–230.
50. Coburn B, Grassl GA, Finlay BB. Salmonella, the host and disease: a brief review. *Immunol. Cell Biol.* 2007;**85**:112–8.
51. Uche IV, MacLennan CA, Saul A. A systematic review of the incidence, risk factors and case fatality rates of invasive nontyphoidal Salmonella (iNTS) disease in Africa (1966 to 2014). *PLoS Negl. Trop. DC.* 2017;**11**:e0005118.
52. Peng H, et al. Controlled enzymatic degradation of poly(ε-caprolactone)-based copolymers in the presence of porcine pancreatic lipase. *Polym. Degrad. Stab.* 2010;**95**:643–50.
53. Gan Z, Fung JT, Jing X, Wu C, Kuliche WK. A novel laser light-scattering study of enzymatic biodegradation of poly(ε-caprolactone) nanoparticles. *Polymer (Guildf)* 1999;**40**:1961–7.
54. Wu C, Jim TF, Gan Z, Zhao Y, Wang S. A heterogeneous catalytic kinetics for enzymatic biodegradation of poly(ε-caprolactone) nanoparticles in aqueous solution. *Polymer (Guildf)* 2000;**41**:3593–7.
55. Kikkawa Y, et al. Tuning the enzymatic hydrolysis of biodegradable polyesters and its application to surface patterning. *J. Mater. Chem. A* 2013;**1**:4667–70.
56. Emmerson KS, Phang JM. Hydrolysis of proline dipeptides completely fulfills the proline requirement in a proline-auxotrophic Chinese hamster ovary cell line. *J. Nutr* 1993;**123**:909–14.
57. Mock WL, Liu Y. Hydrolysis of Picolinylprolines by Prolidase. *J. Biol. Chem.* 1995;**270**:18437–46.
58. Storey RF, Sherman JW. Kinetics and Mechanism of the Stannous Octoate-Catalyzed Bulk Polymerization of ε-Caprolactone. *Macromolecules* 2002;**35**:1504–12.